PCCP

PAPER

Cite this: *Phys. Chem. Chem. Phys.*, 2016, **18**, 8512

Elucidating the role of methyl viologen as a scavenger of photoactivated electrons from photosystem I under aerobic and anaerobic conditions

Tyler Bennett,[ab] Hanieh Niroomand,[ab] Ravi Pamu,[c] Ilia Ivanov,[d] Dibyendu Mukherjee*[abc] and Bamin Khomami*[abc]

Received 4th January 2016,
Accepted 15th February 2016

DOI: 10.1039/c6cp00049e

www.rsc.org/pccp

We present detailed electrochemical investigations into the role of dissolved O_2 in electrolyte solutions in scavenging photoactivated electrons from a uniform photosystem I (PS I) monolayer assembled on alkanethiolate SAM (self-assembled monolayer)/Au surfaces while using methyl viologen (MV^{2+}) as the redox mediator. To this end, we report results for direct measurements of light induced photocurrent from uniform monolayer assemblies of PS I on C9 alkanethiolate SAM/Au surfaces. These measurements, apart from demonstrating the ability of dissolved O_2 in the electrolyte medium to act as an electron scavenger, also reveal its essential role in driving the solution-phase methyl viologen to initiate light-induced directional electron transfer from an electron donor surface (Au) *via* surface assembled PS I trimers. Specifically, our systematic electrochemical measurements have revealed that the dissolved O_2 in aqueous electrolyte solutions form a complex intermediate species with MV that plays the essential role in mediating redox pathways for unidirectional electron transfer processes. This critical insight into the redox-mediated electron transfer pathways allows for rational design of electron scavengers through systematic tuning of mediator combinations that promote such intermediate formation. Our current findings facilitate the incorporation of PS I-based bio-hybrid constructs as photo-anodes in future photoelectrochemical cells and bio-electronic devices.

Introduction

During photosynthesis plants and algae use photosystem I (PS I), a supra-molecular protein complex,[1] to harness solar energy with 100% quantum efficiency. Previous structural and functional studies of trimeric PS I,[1,2] apart from characterizing its shape and dimensions (Fig. 1), have revealed a photo-activated (λ = 680 nm) electron transfer chain. This electron transfer mechanism is mediated by a series of redox reactions initiated at the lumenal side (mid-point potential, E_m (P700/P700$^+$) $\approx$ +0.48 V) and terminated at the stromal side (mid-point potential, E_m (F_A; F_B; F_X) $\approx$ −0.7 V), of the c complex, where the Fe–S clusters are housed. The highly efficient photo-electrochemical activity of PS I has resulted in extensive studies[3,4] towards incorporation of PS I into highly efficient hybrid photochemical and electronic devices.[5–7] However, the first critical step towards achieving this goal requires a highly dense and uniform assembly of the directionally aligned monolayer of PS I complexes on specific electron donor substrates to enable rapid electron transfer from the lumenal to the stromal side of PS I (Fig. 1). To this end, in recent years, significant efforts have been directed towards directional attachment of single PS I trimers,[8] molecular wiring for electron relay,[9] multi-layered PS I assemblies[7,10] using genetically incorporated cysteine tags in PS I mutants along with site specific chemistry to covalently bond with Au,[8] maleimide functionalized carbon nano-tubes (CNT)[5,11] or doped GaAs surfaces.[7] While these approaches are highly effective in directionally immobilizing PS I on various electron donor surfaces, intricate techniques for the synthesis of PS I mutants are required in order to avoid altering the structural and/or functional integrity of the protein. Furthermore, such methods also call for the fabrication of highly specialized and complex nanostructured surfaces. In contrast, in the last several years, systematic and rapid surface assembly of photosynthetic protein complexes (including PS I)[12–16] on

[a] *Materials Research and Innovation Laboratory (MRAIL), Department of Chemical and Biomolecular Engineering, University of Tennessee, Knoxville, TN 37996, USA. E-mail: bkhomami@utk.edu, dmukherj@utk.edu*
[b] *Sustainable Energy Education and Research Center (SEERC), University of Tennessee, Knoxville, TN 37996, USA*
[c] *Department of Mechanical, Aerospace and Biomedical Engineering, University of Tennessee, Knoxville, TN 37996, USA*
[d] *Center for Nanophase Materials Sciences (CNMS), Oak Ridge National Laboratory (ORNL), Oak Ridge, TN 37831, USA*

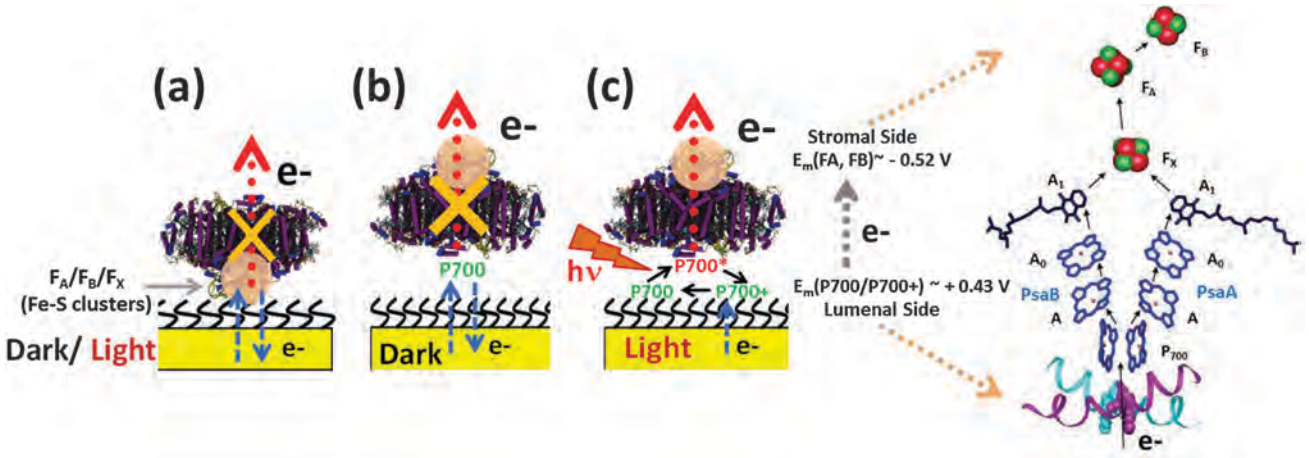

Fig. 1 Schematics of the structure and dimensions of PS I along with the detailed photo-activated (λ = 680 nm) electron transfer pathway initiated on the lumenal side (P700/P700$^+$) and terminated at F_A, F_B, F_X (Fe–S clusters) on the stromal side.[1,2] Relations between electronic activity and different PS I orientations on SAM/Au substrates for: (a) stromal side ($F_A/F_B/F_X$ with Fe–S clusters) facing electrode under dark or, light conditions, (b) lumenal side (P700 reaction center) facing electrode under dark conditions and (c) lumenal side facing electrode under light conditions to promote enhanced electron transfer *via* photoactivated P700*.

alkanethiolate self-assembled monolayer (SAM)/Au substrates have proven to be a simple and highly reproducible method for creating a uniform and dense monolayer of these proteins without denaturing them. Specifically, previous studies have demonstrated that OH-terminated alkanethiolate SAM substrates facilitate directional attachment of PS I with its stromal side facing upwards due to weak hydrogen bonding of the lumenal side of PS I with the terminal OH group.[17,18] Moreover, our recent comprehensive experimental studies of PS I immobilization on electron donor surfaces have revealed that by systematic manipulation of the solution chemistry, *i.e.*, appropriate tuning of surfactant–protein interaction and deposition conditions, gravity driven or electric field assisted deposition techniques can be used to produce a highly dense and uniform monolayer of PS I on a SAM/Au substrate.[13,19,20]

In an effort to understand the photo-activated properties of surface immobilized PS I, recent years have seen a host of electrochemical and photo-electrochemical studies. Many of these studies use dense mono- and multi-layers of PS I directly assembled on Au electrodes[21–23] or, PS I substrates in conjunction with electron scavengers such as methyl viologen (MV) in an electrolyte medium to complete a wet cell circuit.[14,22,24,25] While new redox mediators, both acceptors and donors, are constantly being tested in new concentrations and combinations,[18,24–26] MV has been the most widely used, in part because of its long history of being studied for toxicity effects and electron chain disruption.[27] Specifically, many photoelectrochemical measurements on surface assembled PS I systems have revealed the commonly accepted role of MV^{2+} as the external solution phase electron mediator and dissolved O_2 as the oxidizer to regenerate MV^{2+} from the reduced MV^+. Moreover, recent studies have shown enhanced photocurrents from directionally aligned PS I crystals on substrates as well as, PS I directionally immobilized on SAM/Au surfaces *via* cytochrome cyt_6 mediation.[28] Although such efforts provide valuable data for photo-electrochemical measurements on surface immobilized PS I, they do not provide a clear mechanistic picture for the electron transfer process. Precise morphological characterization of PS I complexes on the electron donor surface is required to determine the contribution of PS I to the electron transfer process. Moreover, the lack of fundamental understanding of the role of external redox mediators in dictating the directional photo-activated electron transfer from PS I trimers prevents any quantitative analysis of the bottlenecks for electron transfer. Thus, the understanding of whether the photocurrent generation is rate limited by mass transfer, redox kinetics, or chemical reaction rates is still an open question. To this end, the critical question that remains unanswered in the current state of the aforementioned research is, "How does the regeneration and migration of an external chemical as the electron scavenger effect photocurrent generation from PS I immobilized on SAM/Au surfaces?"

In this article, detailed electrochemical measurements are used to investigate the role of dissolved O_2 in the electrolyte solution as an electron scavenger as well as its role in activating methyl viologen as a redox mediator during photocurrent generation from a uniform monolayer of photosystem I (PS I) complexes assembled on alkanethiolate SAM (self-assembled monolayer)/Au surfaces. Specifically, results of direct measurements of light induced photocurrent from uniform monolayer assemblies of PS I on C9 alkanethiolate SAM/Au surfaces (refer to Experimental section) are reported. These measurements confirm the ability of dissolved O_2 in the electrolyte to function as a weak electron scavenger for PS I. More importantly, they demonstrate the formation of an intermediate methyl viologen–oxygen complex that directly scavenges the photo-excited electrons from the terminal Fe–S cluster (F_B) of PS I.

Experimental section

The thermophilic cyanobacterium *T. elongatus* BP-1 was grown in 2L airlift fermenters (Bethesda Research Labs, Bethesda MD)

in NTA media.[29] The details of the extraction and purification of the trimeric PS I complexes grown from *T. elongatus* cells are provided elsewhere.[13] Based on spectrophotometer measured chlorophyll concentrations, the concentrations of the extracted PS I trimers were estimated to be around $C_B = 1.42 \times 10^{-5}$ mol L^{-1}. PS I trimers were stored in aliquots of 1.5 ml at −80 °C for future use.

Commercial gold electrodes with 1.6 mm diameter, 2.011 mm^2 working area (BAS Inc.; Model: MF-2014) were cleaned in a three-step process. First, they were treated with base piranha solution (RCA wash with 1 : 1 : 5 volume ratios of $NH_4OH : H_2O_2 : H_2O$) at a temperature of 75 °C for 15 min to remove organic residues. They were then polished with 0.05 micron alumina polish for 3 min. Finally, the electrodes were electrochemically cleaned by running cyclic voltammetry from −400 to +1400 mV *vs.* Ag/AgCl at 200 mV s^{-1} for 25 cycles in 0.1 M H_2SO_4 solution followed by ultra-sonication in isopropanol (99.99% v/v) then de-ionized water for 10 min, and drying in N_2 stream. Commercial glassy carbon (GC) electrodes with 3.0 mm diameter, 7.069 mm^2 working area (BAS Inc.; Model: MF-2012) were used and cleaned only by polishing, sonication, and drying in N_2 stream.

The OH-terminated SAM was formed by immersing the clean Au electrodes in 1 mM 11-mercapto-1-undecanol and 9-mercapto-1-nonanol (97% and 96% purity respectively; purchased from Sigma-Aldrich) in ethanol for 7 days[30] at room temperature in a glove box filled with dry N_2. The SAM/Au electrodes were rinsed in ethanol, sonicated in isopropanol, and dried in dry N_2 stream. Surface immobilization of PS I was carried out by incubating the SAM/Au electrodes for ∼24 h in colloidal suspension of PS I in 200 mM Na-phosphate aqueous buffer (pH = 7.0). Based on our earlier solution chemistry work to tune inter-protein distances that result in "jammed" suspensions,[19] a high PS I concentration of $\sim 1.4 \times 10^{-3}$ mM stabilized with 0.02% w/v (*i.e.*, 2.2 times the critical micellar concentration) of the detergent *n*-dodecyl-β-D-maltoside (DM; purchased from Gold Biotechnology) was specifically chosen to produce uniform, monolayer assemblies of PS I. Since the gold electrodes could not be mounted on the atomic force microscopy (AFM) measuring platforms, AFM topographical characterization for PS I on SAM/Au substrates was carried out on samples prepared using identical solution phase treatments outlined above on Au coated silicon wafers (Au thickness ∼ 100 nm) with a titanium adhesion layer purchased from Platypus Technologies. Multilayer assemblies of PS I on cleaned glassy carbon (GC) electrodes were achieved by drop casting 2.5 μL of stock PS I solution, placed under 30 in. Hg vacuum for 15 min, and rinsed in de-ionized water.

All surface topography images were collected on an AFM instrument from Digital Instruments (Veeco) (Model: NanoScope IIIa) in the tapping mode using a silicon cantilever compatible with softer biological materials (Olympus; Model: AC240TS). The tip had a force constant of 2 N m^{-2} along with a resonant frequency of 70 kHz, and the images were recorded at a scan rate of 0.863 Hz. Surface layer thicknesses were measured using an ellipsometer from DRE-Dr Riss Ellipsometerbau Gmbh (Model: EL X-02C) operating at a laser wavelength of 632.8 nm at an incidence and polarizer angle of 70°. All PS I/SAM/Au systems were analyzed using a three-layer (Au–thiol–PS I) model, where C9 and C11 thiol monolayer thicknesses were assumed to be ∼0.77 and 0.95 nm respectively (based on C–C bond lengths and the brush tilt angle of 30° to the surface normal). As reported in our earlier work[13] and for the ease of data analysis, the refractive indices for surface-assembled PS I and thiols were assumed to be 1.46 altogether.

Electrochemical measurements were conducted using a potentiostat from Bio-Logic (Model: SP-200) operated using the EC-Lab software. A glass electrochemical cell with three-electrode configuration was used that carried a Pt wire counter electrode, the Ag/AgCl (sat. KCl) reference electrode (BAS Inc.; Model: MF-2052 with a reference shift +0.197 V *vs.* NHE) and the Au working electrode with the specific surface treatments (SAM/Au and PS I/SAM/Au electrodes for the controls and specifics respectively). The potential window for all experimental scans was chosen between −0.9 and +0.6 V (*i.e.*, −0.7 to +0.8 V *vs.* NHE) to avoid interference from complex Au oxide peaks above +0.8 V *vs.* NHE. Except where specified, all electrochemical measurements were carried out in a standard electrolyte of 200 mM Na-phosphate aqueous buffer (pH = 7.0) to prevent any protein denaturation. Cyclic voltammetry (CV) data were collected with a scan rate of 200 mV s^{-1}, except where stated at 20 mV s^{-1} and 1000 mV s^{-1}. Chronoamperometry (CA) data were collected at a bias of +0 V *vs.* reference and idled for 20 min before exposing PSI/SAM/Au electrodes to light in 2–5 minute pulses. This potential was chosen to facilitate the photoresponse solely from PS I. It should be mentioned that as bias potentials are shifted further positive or negative, SAM/Au surfaces demonstrated increased photoactivated redox interaction, potentially from stripping of the thiol brushes. This bias is close to the open circuit voltage (OCV) for all tested PS I/SAM/Au constructs, with minor background current shifts. We note here that the OCV shifts at varying solution content and concentrations, as well as upon surface modifications. A constant bias voltage was chosen over OCV to control the energy gap at the electrode surface, which greatly affects the electron kinetics of transfer to and from PSI or methyl viologen (MV). Stepped chronoamperometry data were collected at a series of bias potentials, stepping from −200 to +350 mV *vs.* reference, and exposed to light in 2–5 minute pulses. For all control experiments requiring the purging of the dissolved O_2 from the buffer electrolyte, nitrogen (N_2) gas was bubbled through the solution for 15 min followed by a continuous sheath of N_2 gas being maintained above the solution throughout the experiment. For the oxygen purged runs, O_2 was bubbled through the solution for 30 min, followed by a continuous sheath of O_2 gas flow above. The O_2 levels were measured using an ExStik II Dissolved Oxygen Meter (Model: DO600). 1 mM of methyl violgen (MV) was added as the electron scavenger. All data were measured under dark, room temperature conditions except for the light experiments where the measurements were taken while the working electrodes was under illumination from an LED white-light source (ThorLabs; model: MWWHL3) with a nominal

intensity of 1000 W m^{-2} before being passed through a red filter (λ = 635–650 nm).

Results and discussion

A. Characterization of PS I deposition on SAM/Au substrates

The uniform, monolayer depositions of PS I on SAM/Au substrates as obtained *via* self-assembly from the solution-phase can be observed from the AFM topographical images in Fig. 2a–f. These uniform surface assemblies are achieved through the use of specific PS I/detergent concentration ratios to maintain the individual PS I complexes in colloidal suspension[19] (details are provided in the Experimental section). The AFM images depicted in Fig. 2a and b show that the controls prepared with alkanethiolate SAM/Au surfaces are devoid of PS I. In accordance with earlier studies,[30] the images reveal uniform and dense brush layer formation on the C11-alkanthiolate (C11-thiol) surface (Fig. 2a) as compared to the relatively sparse assembly on the C9-alkanethiolate (C9-thiol) surface (Fig. 2b). Furthermore, AFM images for PS I attachment to SAM/Au surfaces with both C11-thiols and C9-thiols (Fig. 2c and d) indicate a relatively uniform monolayer formation as indicated by the cross-section profile shown in each of the cases (Fig. 2e and f). Typical average protein diameters of d = 32.3 ± 4.5 nm (corresponding to arrows marked on Fig. 2c and d) as well as average heights of h = 8.4 ± 2.3 nm, as indicated in Fig. 2e and f, are recorded from the cross-sectional profiles of PS I deposition on both C11 and C9 alkanethiolate SAM/Au surfaces. These dimensions are commensurate with the expected size of detergent bound PS I

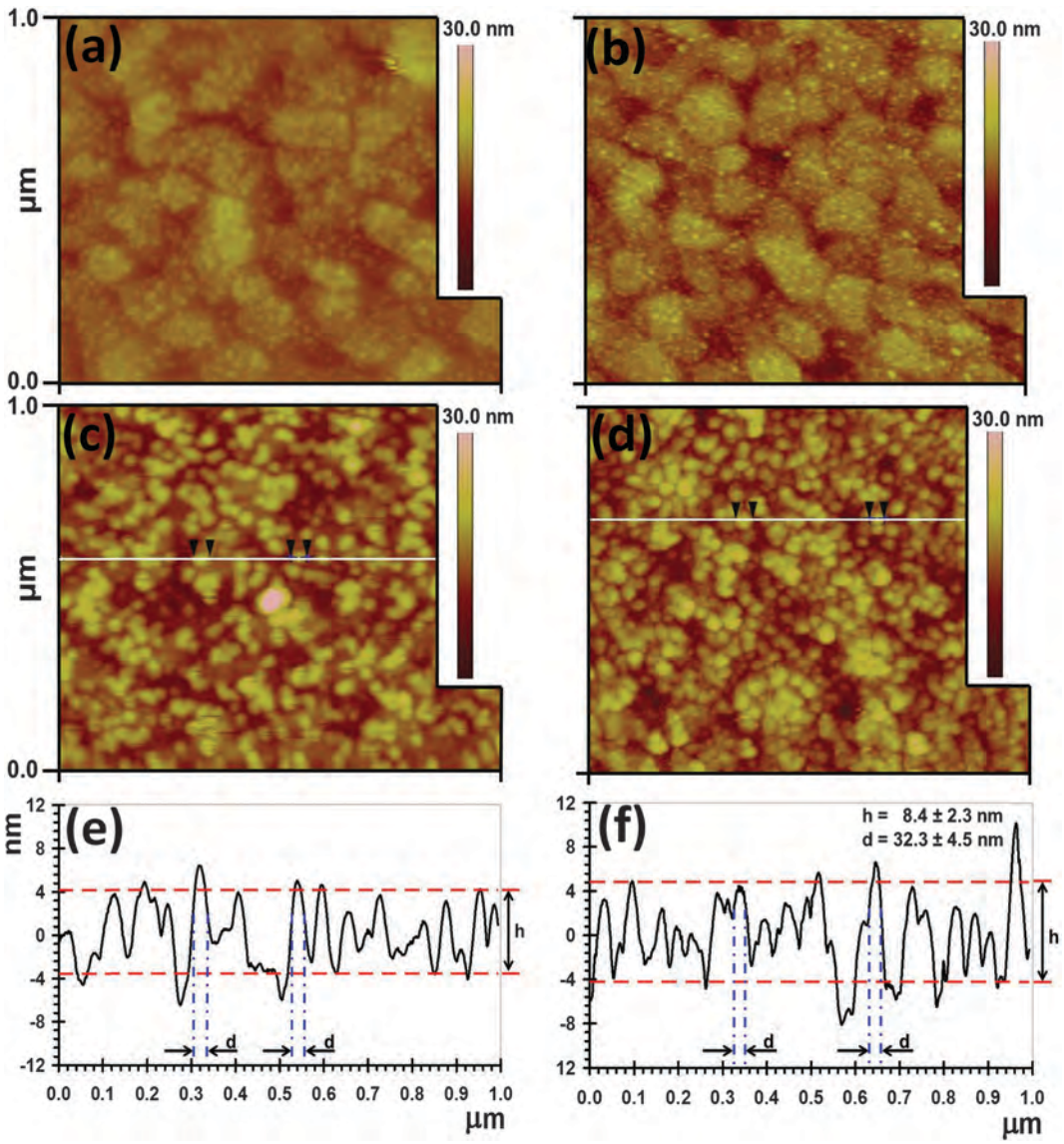

Fig. 2 AFM images showing the surface topographies of: (a) C11-thiol SAM/Au and (b) C9-thiol SAM/Au substrates (background) as well as those for the respective: (c) PS I/C11-thiol SAM/Au and (d) PS I/C9-thiol SAM/Au substrates. Representative cross-sectional surface profiles (e & f) for PS I assembled SAM/Au substrates are shown below the respective AFM images (c & d).

trimeric complexes.[13,19] Additionally, ellipsometry measurements for PS I assembly on C11 and C9 alkanethiolate SAM/Au surfaces indicate the average PS I layer thicknesses to be ~4.2 to 5.1 ± 0.2 nm (*i.e.*, surface coverage of ~50–65%). These measurements, when compared to an average thickness of ~8.0 nm for PS I spheroids with ~9 nm height and an optimal hexagonal packing factor of ~0.9–0.91, indicate that the PS I monolayer considered in this study does not exhibit maximum packing. Such results are in agreement with our earlier studies on PS I deposition from the solution phase.[19] However, for the purpose of the current study it was not critical to attain the PS I monolayer with a maximum packing density as done in our prior studies *via* electric field assisted deposition.

B. Electrochemical measurements to detect PSI activity

Fig. 1 depicts the possible PS I trimer attachments: (1) stromal side ($F_A/F_B/F_X$ with Fe–S clusters as marked by the orange circle) facing the electrode under dark or, light conditions (Fig. 1a); (2) lumenal side (P700 reaction center) facing the electrode under dark conditions (Fig. 1b) and (3) lumenal side facing the electrode under illumination (Fig. 1c). In scenario (1), irrespective of dark or light conditions, there would be only electron exchange between the accessible F_A/F_B redox centers and the Au electrode (electron donor) when biased at the F_A/F_B mid-point potential, but with no soluble electron donor to complete the circuit. In scenario (2), electron transfer cannot occur in the dark, even with upward orientation, as no photo-excited electrons are generated by PS I, causing it to act as an insulator. Only in scenario (3), where PS I trimers assembled on SAM/Au surfaces with upward orientations of $F_X/F_A/F_B$ are illuminated (Fig. 1c), the photoexcitation of P700 → P700* is energetically activated. In turn, the photoexcited reaction center gets oxidized ($P700^* \rightarrow P700^+$) to initiate the electron release to the acceptor chlorophylls, A_0 in the PS I electron transfer chain. The electron deficient and energetically relaxed $P700^+$ scavenges an electron from the Au donor to get reduced as $P700^+ \rightarrow P700$ for the next cycle of photoexcitation, provided a suitable electron scavenger such as methyl viologen (MV) is present to receive the electron from F_B.

Preliminary cyclic voltammetry (CV) measurements on the SAM/Au (controls) and PS I/SAM/Au (specific) electrodes in a Na-phosphate buffer electrolyte (without any external electron scavenger) indicate capacitive (non-faradaic) current built-up due to the presence of dense thiol brushes, in particular for the C11-thiol samples. This background capacitive current masks the signal enhancement in photo-current due to the presence of PS I on SAM electrodes. Thus, once background is subtracted for the control (SAM/Au electrodes) data, negligible CV peaks for PS I redox centers (P700 and Fe–S cluster) were observed. These experiments, in accordance with earlier studies,[14,31] indicate that the CV technique does not possess the sensitivity to clearly identify the electrochemical activities associated with the PS I redox centers from PS I/SAM/Au electrode assemblies. Additionally, chronoamperometry (CA) measurements revealed no discernable photoresponse on the PS I/C11-thiol SAM/Au electrodes. Thus, we believe that the dense brush layer on the C11-thiol/Au electrode, though ideal for better coverage of the PS I monolayer, acts as an insulation barrier that retards electron transfer to the activated P700 reaction center. It should be mentioned here that the accumulation of surface roughness during electrode polishing and cleaning prevents perfectly dense SAM formation, reducing the insulating effects and exposing underlying Au directly to solution. However, because the attachment of PS I is guided by the presence of SAM layers, localized insulation occurs. Hence, all electrochemistry measurements from hereon are reported only for the PS I/C9-thiol SAM/Au samples wherein observable photocurrent from CA measurements is presented.

C. Photocurrent measurements mediated by the presence of dissolved O_2

Chronoamperometry measurements were carried out on PS I/C9-thiol/Au electrodes in light/dark with the addition of MV under both aerobic and anaerobic conditions. We would like to mention here that the aerobic conditions refer to the ambient equilibrium level (~5 mg L^{-1}) of dissolved oxygen (O_2) in buffer electrolyte solutions. Fig. 3a shows that in the presence of MV and dissolved O_2 (Fig. 3a, O_2 present case in blue) a stable photocurrent of ~6 nA cm^{-2} (negative directions as compared to baseline current) is achieved that is comparable to previously

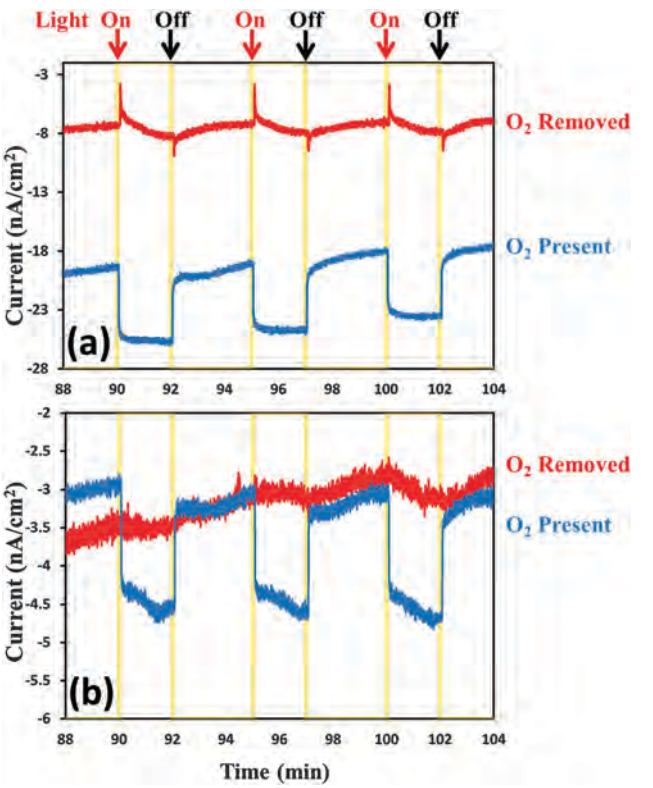

Fig. 3 Chronoamperometry on PS I/C9-thiol SAM/Au electrodes at +0 V bias *vs.* Ag/AgCl under illumination (λ = 635–650 nm) under both aerobic (O_2 present; blue line) and anaerobic (O_2 absent; red line) conditions with: (a) 1 mM methyl viologen (MV) added as a charge carrier showing suppression of photocurrent with O_2 removed; (b) all charge carrier removed from solution, showing small direct scavenging of electrons by O_2.

reported values from CA measurements on PS I/C6-thiol/Au electrodes.[14] While a mixed orientation of PS I complexes is expected on SAM/Au surfaces, the photoresponse in Fig. 3a demonstrates that the dominant electron transfer pathway involves the reduction of photo-excited P700*/$P700^+$ by electrons from the Au donor. Current understandings of the electron transfer mechanism assume the final oxidation of F_B^- (redox potential ~ -0.53 V *vs.* NHE) at the stromal side of PS I is directly mediated by the electron being scavenged by MV^{2+} (redox potential ~ -0.45 V *vs.* NHE). However, upon the removal of all dissolved O_2 through systematic purging with nitrogen (N_2) in the electrolyte solution, this photoresponse shifts to a sharp positive spike in current (see Fig. 3a, O_2 removed case in red). Such a photocurrent spike is indicative of electron transfer into the Au surface *via* oppositely oriented PS I, which rapidly diminishes due to the unavailability of suitable charge carriers in solution to donate electrons to $P700^+$.

In an effort to understand the exact role of O_2 in the electron mediation from PS I immobilized on SAM/Au substrates, CA measurements were carried on identical PS I/SAM/Au electrodes in buffer electrolyte solution devoid of any MV. As expected, Fig. 3b shows no photoresponse in the absence of oxygen (O_2 removed case in red). However, O_2 in the solution alone is able to scavenge electrons from F_B^- to produce a steady negative photocurrent of ~ 1.5 nA cm^{-2} even in the absence of MV as the charge carrier (O_2 present case in blue). This confirms, a hypothesis put forward in an earlier study,[26] that O_2 in solution alone can directly scavenge electrons from F_B^-. However, the interaction between dissolved O_2 and MV still remains unclear, since there is a 4-fold increase in photocurrent when MV is added under aerobic conditions as compared to the corresponding photoresponse under anaerobic conditions. To enhance our understanding of the role of O_2 in scavenging the photoactivated electrons, we further ask the question: if removal of oxygen from the system suppresses the photocurrent response, then does increasing the oxygen content enhance it? To this end, fully purged solution was subsequently oxygenated in incremental stages by bubbling a 70%N_2/30%O_2 gas, while recording the photoresponse as dissolved O_2 content increased. As shown in Fig. 4, this photocurrent peaks at ~ 5 mg L^{-1}, which incidentally coincides with the ambient level of dissolved O_2 found in freshly deionized Millipore water. The subsequent decrease in photocurrent is attributed to oxygen reacting with the sulfur group of thiol to strip the SAM and remove PS I from the surface. Thus for given amounts of MV and PS I present, the normal level of oxygen found in our solution is sufficient to maximize the photoresponse. Although our observations confirm the catalytic role of dissolved O_2 in activating the solution-phase MV to effectively scavenge the electrons, they do not provide a fundamental understanding of the mechanism that makes the presence of dissolved O_2 imperative to sustained photocurrents.

D. Electrochemical measurements indicative of an intermediate redox species

The commonly accepted mechanism[32] of the reduction of solution-phase MV^{2+} by F_B^- ($MV^{2+} \rightarrow MV^+$) followed by their regeneration due to oxidation by O_2 ($MV^+ \rightarrow MV^{2+}$) appears insufficient to explain the behavior shown in Fig. 3a. To further elucidate the role of O_2, let us assume that the aforementioned and commonly accepted electron transfer mechanism holds true. In the absence of dissolved O_2, one would expect a negative photocurrent spike which would quickly decay. The substantial (1 mM) population of MV^{2+} in the immediate vicinity of the PS I layer should still scavenge electrons initially. However, without O_2 to regenerate the MV^{2+}, available scavenger species at the surface would be exhausted and photocurrent intensity would diminish. In contrast, the photocurrents observed in Fig. 3a in the absence of O_2, with MV as the electron scavenger in solution, show a sharp positive response that quickly decays in time. While such observations provide weak indication of the possibility of MV^+ donating to reduce $P700^+$, as proposed by others,[33] it raises questions about the current picture of PS I–MV interactions.

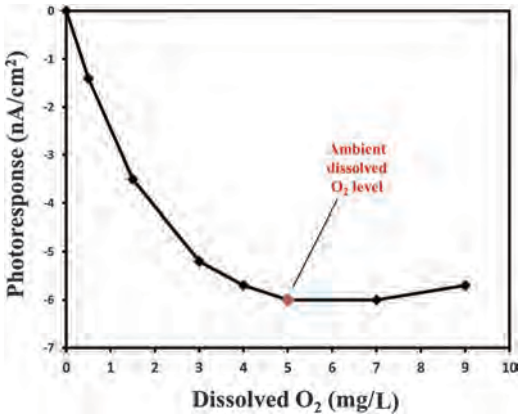

Fig. 4 Net photocurrent change in series of chronoamperometry on PS I/C9-thiol SAM/Au electrodes at +0 V bias *vs.* Ag/AgCl under illumination (λ = 635–650 nm) with 1 mM methyl viologen. O_2 concentration heavily regulates the scavenging of electrons from PS I. For the given concentration of MV, adding oxygen beyond the ambient amount present in Millipore deionized water did not further increase the photoresponse of PS I.

To this end, cyclic voltammetry (CV) measurements on PS I/SAM/Au electrodes in buffer electrolytes carrying solution-phase MV, both with and without oxygen, reveal a new electrochemical pathway for the electron transfer process. In Fig. 5, dark CV scans at 200 mV s^{-1} in electrolytes containing MV, but purged of all O_2, demonstrate a repeatable, stable trace over 20 cycles with the well-established redox peaks (-450 mV *vs.* NHE)[34] for $MV^{2+} \leftrightarrow MV^+$. However, the addition of O_2 not only brings the expected increase in cathodic current at negative potentials due to electrons being scavenged form the electrode surface, but also introduces a new irreversible peak indicating the reduction of an unknown solution-phase chemical species at ~ -325 mV *vs.* NHE. This peak diminishes with successive cycles, indicating an irreversible electron transfer process which results from the depletion of the aforementioned species at the electrode surface. This peak reappears slowly over time between scans and more quickly if the solution is shaken to promote O_2 diffusion from the air, which indicates the formation of a metastable methyl viologen–oxygen complex [MVO*]. In order

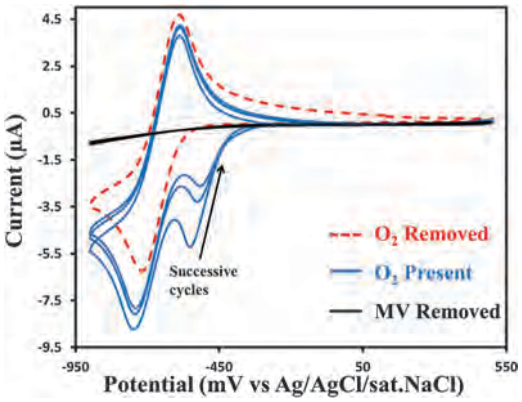

Fig. 5 Cyclic Voltammetry scans at 200 mV s^{-1} on PS I/C9-thiol SAM/Au electrodes *vs.* Ag/AgCl in the dark with 1 mM MV in solution. When purged with nitrogen to remove all oxygen, the scans exhibited a stable repeated single redox peak for MV at the expected potential of ~−0.65 V. When oxygen is introduced, an irreversible redox peak appears that diminishes in magnitude upon successive scans, which is attributed to the reduction of the metastable methyl viologen–oxygen complex.

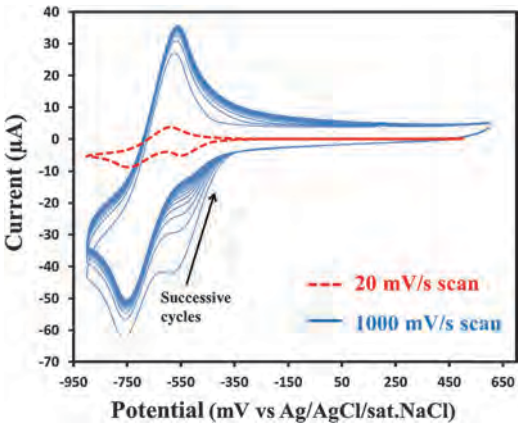

Fig. 6 Cyclic Voltammetry scans on PS I/C9-thiol SAM/Au electrodes *vs.* Ag/AgCl in dark with 1 mM MV in solution in aerobic conditions. Immediately stable trace at 20 mV s^{-1} scan and greatly diminishing reduction peak at 1000 mV s^{-1} scan indicates a methyl viologen–oxygen complex being formed in solution and consumed at the electrode surface.

to determine if this [MVO*] species was created at the electrode surface, CV scans at greatly reduced and increased scan rates were repeated (Fig. 6). The slowest scan rate of 20 mV s^{-1} indicated a stable trace, while the fastest scan rate of 1000 mV s^{-1} greatly amplified the trend of the disappearing peak at ~−325 mV (*vs.* NHE) with successive cycles. Such measurements indicate that this species is generated in the bulk solution and reduced at the surface. To further understand this process, we specifically carried out CV scans while purging the MV solution with additional pure O_2 (Fig. 7). It is observed here that the distinct shoulder features of the individual redox peaks become less distinguishable since the excessive dissolved oxygen content provides a significant background reduction current. However, it can still be clearly seen that the specific redox peak for this [MVO*] complex significantly increases in both magnitude and breadth. Simultaneously, the peak to peak height difference

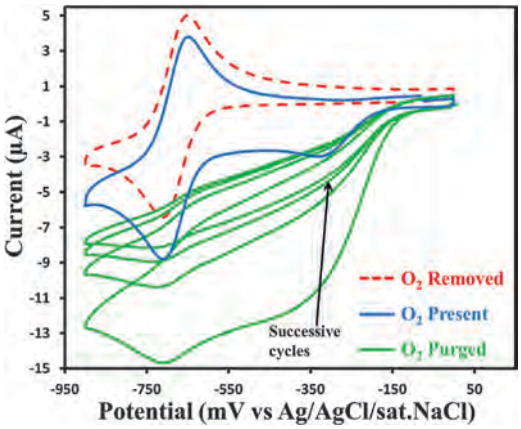

Fig. 7 Cyclic Voltammetry scans at 200 mV s^{-1} on PS I/C9-thiol SAM/Au electrodes *vs.* Ag/AgCl in dark with 1 mM MV in solution. When purged with nitrogen to remove all oxygen, the scans exhibited a stable repeated single redox peak for MV at the expected potential of ~−0.65 V. When pure oxygen is bubbled through the solution, the irreversible redox peak appears grows in magnitude, while the distinguishable MV^+/MV^{2+} pair diminishes by ~50% peak to peak height.

for the MV^+/MV^{2+} redox couple reduces by ~50% after the first cycle. This reduction would be expected if the increased O_2 concentration has shifted the equilibrium concentration in favor of the [MVO*] complex, reducing the concentration of MV^{2+} species present. In successive cycles, the MV^+/MV^{2+} redox couple peak stabilizes in magnitude, while the shoulder feature continues to diminish as this [MVO*] complex is irreversibly consumed upon reduction. While these results clearly indicate the spontaneous formation of the aforementioned complex before any interaction with PS I, as also hypothesized before, the unanswered question here is whether the concentration of this complex is the limiting factor that inhibits the electron transport chain of substrate → PS I → the final solution-phase scavenger.

In an effort to investigate the ability of methyl viologen to scavenge electrons directly in the absence of oxygen, we sought to augment the observed photocurrent effects at varying electrode bias voltages. However, the thiol SAM/Au formation proves to be unstable when the electrodes are exposed to a wider range of bias potentials over long periods of times (as required for CA experiments), especially deteriorating rapidly at negative overpotentials. Thus we drop cast PS I directly onto glassy carbon electrodes (GCE) to form multilayers that are stable over a much larger range of bias potentials and for longer periods of time (Fig. 8). Applying a negative bias potential increases the electron energy at the electrode surface, thereby facilitating the charge transfer to $P700^+$. If MV^{2+} is the primary species scavenging electrons from F_B^-, we should see a significant increase in the magnitude of the photocurrent with decreasing bias potential on the electrodes. However, in the absence of O_2 (Fig. 8), the net photocurrent values at bias potentials <100 mV (*vs.* NHE) are significantly suppressed as compared to the corresponding values in the presence of oxygen. Added to this, the characteristic trend for the photoresponse curve at −100 mV bias potential in Fig. 9.a indicates

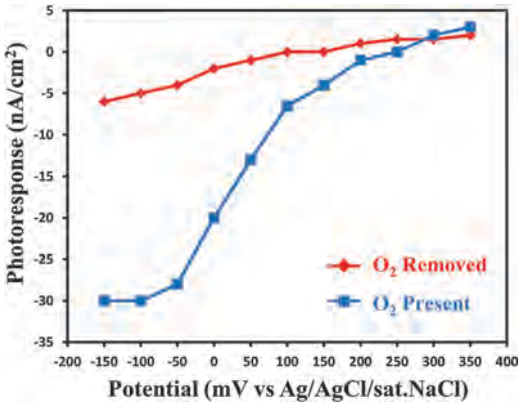

Fig. 8 Net photocurrent change in series of continuous chronoamperometry biased steps on dropcast PS I/GC electrodes under illumination (λ = 635–650 nm) with 1 mM methyl viologen (MV) added as a charge carrier under aerobic and anaerobic conditions.

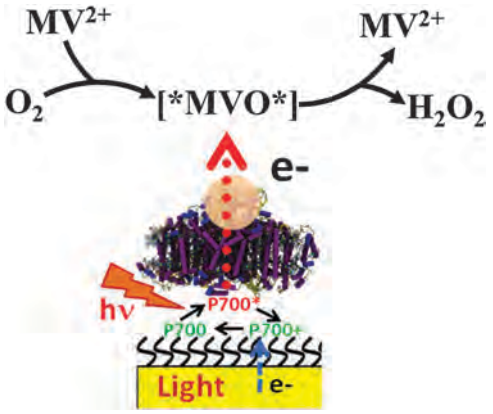

Fig. 10 Proposed series of events with MV reacting with oxygen to form an intermediate, which is the species responsible for direct electron scavenging, in contrast to the understanding of MV^{2+} directly scavenging and subsequently being regenerated by O_2.

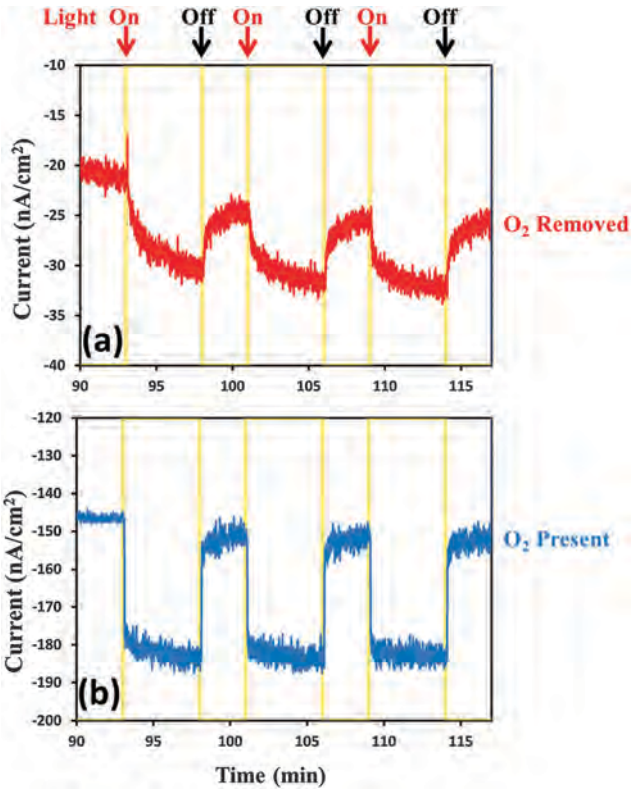

Fig. 9 Chronoamperometry on dropcast PS I/GC electrodes at −100 mV bias *vs.* Ag/AgCl under illumination (λ = 635–650 nm) with 1 mM methyl viologen (MV) added as charge carrier under (a) anaerobic (O_2 removed, red line) and (b) aerobic (O_2 present; blue line) showing suppression of photocurrent with O_2 removed. Even at negative overpotentials, the distinct characteristic differences in the photoresponse curves indicates a separate species from MV^{2+} involved in electron scavenging.

the same response as previously observed for the 0 V bias potential case. Thus, we observe an immediate and stable negative photoresponse in the presence of O_2 (Fig. 9b). However, in the absence of O_2, we only see a slower decay towards a negative response (Fig. 9a). To sum it up, even at negative overpotentials, no sharp photoresponse indicative of any direct electron scavenging by MV^{2+} alone was observed.

Our explanation for the aforementioned phenomena is that MV^{2+} first reacts with O_2 to form a new intermediate complex, [MVO*]. This species then directly scavenges the electron from PS I and is subsequently regenerated to MV^{2+} while producing H_2O_2, as depicted in Fig. 10. This is in contrast with the previous understanding that MV^{2+} directly takes up an electron from PS I to then react with O_2 and form H_2O_2. Previous work has pointed towards a large number of possible intermediates: $[MV^+O^-]$, [MVO], $[MVO^+]$, $[MV(O)_2]$, $[MV^+O_2^-]$, $[MV(OH)_2]$,[35] along with the possibility of directly photogenerated $[MV^{+\bullet}]$.[36] Due to the ephemeral nature of such solution-phase complex formation, it is outside the scope of this work to propose the exact molecular structure of the intermediate species, except to say that it is an electron-starved species which reacts upon reduction. With the aim of choosing suitable electron scavengers through a fundamental understanding of the electron transfer pathways, it is sufficient to replace the existing model of MV^{2+} scavenging and subsequently donating the electron to O_2 with a more accurate model as depicted schematically in Fig. 10. Thus, when using MV as an electron scavenger in the presence of oxygen, the emergence of this intermediate species as the primary electron scavenger makes it more rational to consider the effective redox potential of the scavenger as −325 mV *vs.* NHE instead of the previously assumed −450 mV.

Conclusions

Chronoamperometry measurements under light and dark conditions reveal the mechanistic picture behind the electrochemical pathway mediated by methyl viologen for the electron transport from the stromal F_A/F_B terminal of PS I (the ones that are directionally oriented) to the counter electrode in solution. Specifically, our experiments reveal the critical role of solution-phase dissolved O_2 concentrations in producing an intermediate complex (MVO*), heretofore not accounted for, facilitates the

electron scavenging mechanism in the presence of MV. Thus, the rate limiting step in the kinetics of photocurrent generation from PS I/SAM/Au systems is directly related to the rate of formation of this complex, as evidenced by the non-linear increase in photocurrent density with increasing dissolved O_2 concentrations.

The proposed model for the electron transfer pathway from our current findings paves the way for rational design of PS I wet cells that use combinations of well-known mediators such as methyl viologen and ferrocyanide,[24] or methyl viologen and an osmium base.[18] In the framework of such a model, the redox potential for electron scavenging by the most successful and widely used methyl viologen needs to be re-adjusted from −450 mV to −325 mV *vs.* NHE. Such observations provide critical insight into the optimization of the energetics of electron transport pathways from PS I to a soluble carrier, a solid-state electrode, or bound catalysts in future photoactivated bio-hybrid energy harvesting constructs.

Acknowledgements

B. K. would like to acknowledge the National Science Foundation (EPS-1004083) and the Gibson Family Foundation. A portion of this research was conducted at the Center for Nanophase Materials Sciences (CNMS), which is sponsored at Oak Ridge National Laboratory by the Scientific User Facilities Division, Office of Basic Energy Sciences, U.S. Department of Energy.

References

1 N. Nelson and C. F. Yocum, Structure and Function of Photosystems I and Ii, *Annu. Rev. Plant Biol.*, 2006, **57**, 521–565.
2 P. Jordan, P. Fromme, H. T. Witt, O. Klukas, W. Saenger and N. Krauss, Three-Dimensional Structure of Cyanobacterial Photosystem I at 2.5 Angstrom Resolution, *Nature*, 2001, **411**, 909–917.
3 R. E. Blankenship, *et al.*, Comparing Photosynthetic and Photovoltaic Efficiencies and Recognizing the Potential for Improvement, *Science*, 2011, **332**, 805–809.
4 D. A. LaVan and J. N. Cha, Approaches for Biological and Biomimetic Energy Conversion, *Proc. Natl. Acad. Sci. U. S. A.*, 2006, **103**, 5251–5255.
5 I. Carmeli, M. Mangold, L. Frolov, B. Zebli, C. Carmeli, S. Richter and A. W. Holleitner, A Photosynthetic Reaction Center Covalently Bound to Carbon Nanotubes, *Adv. Mater.*, 2007, **19**, 3901–3905.
6 R. Das, *et al.* Integration of Photosynthetic Protein Molecular Complexes in Solid-State Electronic Devices, *Nano Lett.*, 2004, **4**, 1079–1083.
7 L. Frolov, O. Wilner, C. Carmeli and I. Carmeli, Fabrication of Oriented Multilayers of Photosystem I Proteins on Solid Surfaces by Auto-Metallization, *Adv. Mater.*, 2008, **20**, 263–266.
8 L. Frolov, Y. Rosenwaks, C. Carmeli and I. Carmeli, Fabrication of a Photoelectronic Device by Direct Chemical Binding of the Photosynthetic Reaction Center Protein to Metal Surfaces, *Adv. Mater.*, 2005, **17**, 2434–2437.
9 B. Terasaki, *et al.*, Plugging a Molecular Wire into Photosystem I: Reconstitution of the Photoelectric Conversion System on a Gold Electrode, *Angew. Chem.*, 2009, **48**, 1585–1587.
10 G. LeBlanc, G. Chen, E. A. Gizzie, G. K. Jennings and D. E. Cliffel, Enhanced Photocurrents of Photosystem I Films on P-Doped Silicon, *Adv. Mater.*, 2012, **24**, 5959–5962.
11 S. M. Kaniber, M. Brandstetter, F. C. Simmel, I. Carmeli and A. W. Holleitner, On-Chip Functionalization of Carbon Nanotubes with Photosystem I, *J. Am. Chem. Soc.*, 2010, **132**, 2872–2873.
12 M. Kondo, Y. Nakamura, K. Fujii, M. Nagata, Y. Suemori, T. Dewa, K. Lida, A. T. Gardiner, R. J. Cogdell and M. Nango, Self-Assembled Monolayer of Light-Harvesting Core Complexes from Photosynthetic Bacteria on a Gold Electrode Modified with Alkanethiols, *Biomacromolecules*, 2007, **8**, 2457–2463.
13 D. Mukherjee, M. May, M. Vaughn, B. D. Bruce and B. Khomami, Controlling the Morphology of Photosystem I Assembly on Thiol-Activated Au Substrates, *Langmuir*, 2010, **26**, 16048–16054.
14 M. Ciobanu, H. A. Kincaid, V. Lo, A. D. Dukes, G. K. Jennings and D. E. Cliffel, Electrochemistry and Photoelectrochemistry of Photosystem I Adsorbed on Hydroxyl-Terminated Monolayers, *J. Electroanal. Chem.*, 2007, **599**, 72–78.
15 H. A. Kincaid, T. Niedringhaus, M. Ciobanu, D. E. Cliffel and G. K. Jennings, Entrapment of Photosystem I within Self-Assembled Films, *Langmuir*, 2006, **22**, 8114–8120.
16 B. S. Ko, B. Babcock, G. K. Jennings, S. G. Tilden, R. R. Peterson, D. Cliffel and E. Greenbaum, Effect of Surface Composition on the Adsorption of Photosystem I onto Alkanethiolate Self-Assembled Monolayers on Gold, *Langmuir*, 2004, **20**, 4033–4038.
17 I. Lee, J. W. Lee and E. Greenbaum, Biomolecular Electronics: Vectorial Arrays of Photosynthetic Reaction Centers, *Phys. Rev. Lett.*, 1997, **79**, 3294–3297.
18 A. K. Manocchi, D. R. Baker, S. S. Pendley, K. Nguyen, M. M. Hurley, B. D. Bruce, J. J. Sumner and C. A. Lundgren, Photocurrent Generation from Surface Assembled Photosystem I on Alkanethiol Modified Electrodes, *Langmuir*, 2013, **29**, 2412–2419.
19 D. Mukherjee, M. May and B. Khomami, Detergent-Protein Interactions in Aqueous Buffer Suspensions of Photosystem I (Ps I), *J. Colloid Interface Sci.*, 2011, **358**, 477–484.
20 D. Mukherjee, M. Vaughn, B. Khomami and B. D. Bruce, Modulation of Cyanobacterial Photosystem I Deposition Properties on Alkanethiolate Au Substrate by Various Experimental Conditions, *Colloids Surf., B*, 2011, **88**, 181–190.
21 P. N. Ciesielski, F. M. Hijazi, A. M. Scott, C. J. Faulkner, L. Beard, K. Emmett, S. J. Rosenthal, D. Cliffel and G. K. Jennings, Photosystem I – Based Biohybrid Photoelectrochemical Cells, *Bioresour. Technol.*, 2010, **101**, 3047–3053.

22 A. K. Manocchi, D. R. Baker, S. S. Pendley, K. Nguyen, M. M. Hurley, B. D. Bruce, J. J. Sumner and C. A. Lundgren, Photocurrent Generation from Surface Assembled Photosystem I on Alkanethiol Modified Electrodes, *Langmuir*, 2013, **29**, 2412–2419.
23 E. A. Gizzie, G. LeBlanc, G. K. Jennings and D. E. Cliffel, Electrochemical Preparation of Photosystem I–Polyaniline Composite Films for Biohybrid Solar Energy Conversion, *ACS Appl. Mater. Interfaces*, 2015, **7**, 9328–9335.
24 G. Chen, G. LeBlanc, G. K. Jennings and D. E. Cliffel, Effect of Redox Mediator on the Photo-Induced Current of a Photosystem I Modified Electrode, *J. Electrochem. Soc.*, 2013, **160**, H315–H320.
25 Y. Yamanoi, N. Terasaki, M. Miyachi, Y. Inoue and H. Nishihara, Enhanced Photocurrent Production by Photosystem I with Modified Viologen Derivatives, *Thin Solid Films*, 2012, **520**, 5123–5127.
26 A. Badura, D. Guschin, T. Kothe, M. J. Kopczak, W. Schuhmann and M. Roegner, Photocurrent Generation by Photosystem 1 Integrated in Crosslinked Redox Hydrogels, *Energy Environ. Sci.*, 2011, **4**, 2435–2440.
27 Z. E. Suntres, Role of Antioxidants in Paraquat Toxicity, *Toxicology*, 2002, **180**, 65–77.
28 K. R. Stieger, S. C. Feifel, H. Lokstein and F. Lisdat, Advanced Unidirectional Photocurrent Generation Via Cytochrome C as Reaction Partner for Directed Assembly of Photosystem I, *Phys. Chem. Chem. Phys.*, 2014, **16**, 15667–15674.
29 J. F. Talling and D. Driver, in *Primary Productivity Measurements, Marine and Freshwater*, ed. M. Doty and U. A. E. Commission, Washington, DC, 1963, vol. TID 7633.
30 J. C. Love, L. A. Estroff, J. K. Kriebel, R. G. Nuzzo and G. M. Whitesides, Self-Assembled Monolayers of Thiolates on Metals as a Form of Nanotechnology, *Chem. Rev.*, 2005, **105**, 1103–1170.
31 O. Kievit and G. W. Brudvig, Direct Electrochemistry of Photosystem I, *J. Electroanal. Chem.*, 2001, **497**, 139–149.
32 C. L. Bird and A. T. Kuhn, Electrochemistry of the Viologens, *Chem. Soc. Rev.*, 1981, **10**, 49–82.
33 C. N. Kozi Asada, Ulrich Heber and Ulrich Schreiber, Methyl Viologen-Dependent Cyclic Electron Transport in Spinach Chloroplasts in the Absence of Oxygen, *Plant Cell Physiol.*, 1990, **31**, 557–564.
34 L. M. a. E. S. Hill, The Viologen Indicators, *J. Gen. Physiol.*, 1933, **16**, 859–873.
35 E. J. Nanni, C. T. Angelis, J. Dickson and D. T. Sawyer, Oxygen Activation by Radical Coupling between Superoxide Ion and Reduced Methyl Viologen, *J. Am. Chem. Soc.*, 1981, **103**, 4268–4270.
36 T. W. Ebbesen, G. Levey and L. K. Patterson, Photoreduction of Methyl Viologen in Aqueous Neutral Solution without Additives, *Nature*, 1982, **298**, 545–548.